Medical Engineering and Physics 67 (2019) 66–72

Contents lists available at ScienceDirect

Medical Engineering and Physics

journal homepage: www.elsevier.com/locate/medengphy

Inline flow sensor for ventriculoperitoneal shunts: Experimental evaluation in swine

Chuchu Qin[a], Albert H. Olivencia-Yurvati[b,c], Arthur G. Williams Jr.[c], Dane Eskildsen[d], Robert T. Mallet[c], Purnendu K. Dasgupta[a,*]

[a] Department of Chemistry and Biochemistry, University of Texas at Arlington, Arlington, TX 76019-0065, United States
[b] Department of Medical Education, University of North Texas Health Science Center, Fort Worth, TX 76107-2699, United States
[c] Department of Physiology and Anatomy, University of North Texas Health Science Center, Fort Worth, TX 76107-2699, United States
[d] Department of Medical Education, Texas College of Osteopathic Medicine, University of North Texas Health Science Center, Fort Worth, TX 76107-2699, United States

ARTICLE INFO

Article history:
Received 15 August 2018
Revised 10 January 2019
Accepted 17 March 2019

Keywords:
Hydrocephalus
Ventriculoperitoneal shunt
Flow sensor
Bidirectional thermal transducer

ABSTRACT

Shunts are commonly employed to treat hydrocephalus, a severe central nervous disease caused by the buildup of cerebrospinal fluid in the brain. These shunts divert excessive cerebrospinal fluid from brain ventricles to other body cavities, thereby relieving the symptoms. However, these shunts are highly prone to failure due to obstruction from cellular debris, leading to cerebrospinal fluid accumulation in the brain and exacerbation of neurological symptoms. Therefore, there is a clinical need for a reliable, non-invasive method of monitoring shunt performance. Recently, a simple inline flow sensor was reported for monitoring ventriculoperitoneal shunting of cerebrospinal fluid in hydrocephalus treatment. The present work aimed to evaluate performance of the device in an animal model of hydrocephalus. Sensor-equipped shunt tubes were placed in anesthetized, juvenile swine. The flows reported by the sensor were compared with gravimetric flow measurements. Robust correlations ($r \approx 0.87–0.96$) between the gravimetric and sensor-reported flows were obtained in 4 of the 6 experiments. The mean slope of the linear relationship of the gravimetrically determined vs. sensor flow rates was 0.98 ± 0.09 in the 6 experiments, indicating the sensor accurately reported shunt flows up to 35 ml/h. The sensor responded immediately to abrupt flow changes following cerebroventricular fluid injections. Minor hardware problems were identified and corrected. These experiments provide practical guidance for future preclinical testing of the device.

1. Introduction

Hydrocephalus, a disorder caused by the buildup of cerebrospinal fluid (CSF) in the cerebral ventricles, affects approximately 0.2% of live births [1,2] and is responsible for nearly 40,000 annual hospital admissions in the United States [3]. The syndrome also affects adults, especially stroke patients over the age of 60 [4]. The major etiologies of hydrocephalus are obstruction to the CSF outflow tract [5], overproduction [6] or decreased reabsorption [7] of CSF, ischemic stroke [4] and intracerebral hemorrhage [8]. The accumulation of CSF increases intracranial pressure and dilates the ventricles, often resulting in life-threatening complications such as lethal brain herniation. Untreated, hydrocephalus can culminate in permanent brain damage and even death [9].

Hydrocephalus is most commonly treated by surgical placement of shunts that divert subdural CSF drainage from the cerebral ventricles to the peritoneal cavity, thereby stabilizing intracranial pressure [10]. Although effective when initially installed, 40% of these shunts fail within the first year of placement, and an additional 5% fail in each subsequent year [11–13]. Mechanical shunt failure can occur due to obstruction or fracture of the tubing, or dislodging of the shunt from the cerebral ventricle. Without drainage, CSF accumulates rapidly within the ventricles and raises pressure in the cranial vault; thus, shunt failure is a medical emergency requiring prompt surgical intervention.

Current methods for evaluating shunt performance employ static imaging techniques, e.g. computed tomography or magnetic resonance imaging, and plain radiography of the shunt pathway.

* Corresponding author.
E-mail address: Dasgupta@uta.edu (P.K. Dasgupta).

https://doi.org/10.1016/j.medengphy.2019.03.010

Such techniques are not without limitations. For example, radiographic shunt series expose the patient to radiation, and must be repeated if the shunt series images are poor [14]. Moreover, static imaging methods can be expensive and have limited diagnostic value. Shunt flow and CSF pressure can also be assessed by shunt tapping, but this method requires exposure of the shunt architecture, raising infection risks [15].

Another method for diagnosing shunt failure utilizes a device called ShuntCheck, specifically designed to assess CSF flow in the shunt. This device detects the presence or absence of flow, but cannot quantify flow rate. CSF only flows through the shunt when intracerebral pressure is high enough to open a check valve integral to the shunt tube. Because shunt flow is phasic and episodic, an absence of flow does not necessarily indicate shunt failure [16]. The device therefore cannot differentiate shunt failure from normal periods of shunt stasis. Furthermore, as the ShuntCheck system only gives qualitative flow information, it cannot detect gradually developing shunt failures, e.g. due to biofouling [16].

As the ShuntCheck is the only FDA approved device for the detection of shunt flow, there is an urgent need for development of flow sensors which provide quantitative flow information. To address this need, a novel in-line flow sensor was developed, capable of monitoring CSF flow over time and, importantly, providing quantitative information about shunt flow. This study evaluated the sensor's ability to quantify CSF flows originating from the cerebral ventricles. Experiments were conducted in domestic pigs, which exhibit cerebroventricular architecture similar to patients undergoing shunt installation or replacement.

2. Methods

2.1. Inline shunt flow monitor for swine testing

The principle of the thermistor-based shunt flow monitor evaluated in this study was presented in a recent report [17]. In brief, a single micro thermistor (0.5×2 mm; $R_{30\,^{\circ}C} = 17.48$ kΩ, temperature coefficient = −0.85%/ °C; SEMITEC 223Fμ5183-15U004, www.mouser.com) was used alternately as a heater and as a temperature sensor. In the sensing mode, the thermistor is part of a Wheatstone bridge that measures resistance; the bridge output voltage is directly related to the temperature. Next the thermistor is disconnected from the bridge and a short duration (5 s) voltage pulse is applied to heat the adjacent fluid by ~2 °C, and then the circuit reverts to temperature measurement. At 30 °C the sensing and heating currents through the thermistor are 80 and 560 μA, respectively. The rate of shunt flow past the thermistor is derived from the rate of shunt fluid cooling. The temperature difference of the thermistor before and after the heat pulse (corresponding to the difference in the bridge output voltage, ΔV, immediately before and after the pulse) is sufficient to determine the flow (F). At a given F, the temperature difference also is affected by the initial temperature of the thermistor, which is revealed by the initial bridge voltage (V_i).

The sensor configuration is shown in Fig. 1. Minor modifications were made to the original design [17] to improve compactness and portability. The sensor cell was pre-calibrated to detect flows between 0–52.5 mL/h at 32–39 °C (experiment 1), 26–34 °C (experiments 2–7) or 28–32 °C (experiments 8). This flow range fully encompasses CSF flow rate ranges reported in hydrocephalus patients [18,19]. Three thermistors of the same design were used during the present experiments: Experiments 1–4 were conducted with the first thermistor, experiments 5–7 with the second, and experiment 8 with the third.

Each sensor was individually calibrated *in-vitro* and the calibration pertaining to that particular device was applied during the experiment to derive flow values from the thermistor read-

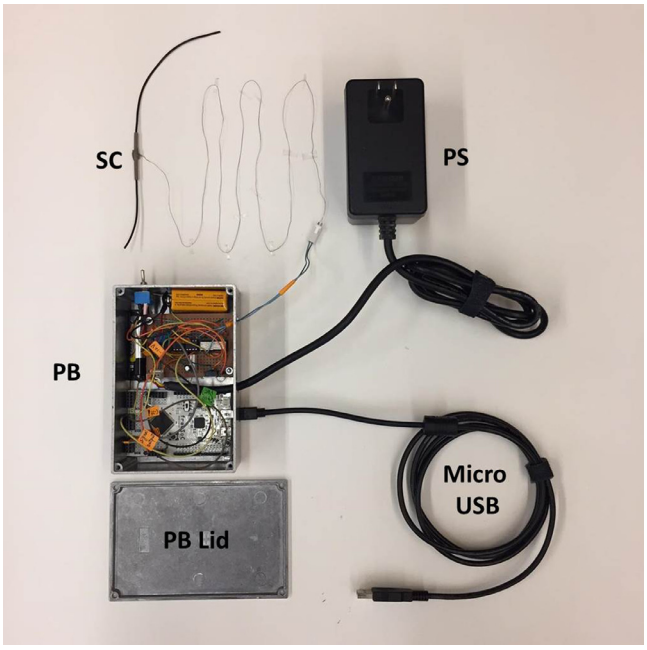

Fig. 1. Sensor instrumentation. SC, sensor cell: thermistor is inserted in a PEEK tube and secured with hot adhesive. Two PTFE tubes connect to the silicone shunt. PB, project box with circuit board and microcontroller inside; PB Lid, project box lid; PS, power supply for circuit board. The micro USB cable is used for instrumental control and interfaces with a computer for data acquisition.

out. The calibration equations for the three sensors were as follows (Fig. S1–3):

$$Sensor\ 1:\ F = 8.138 \times 10^{-5} \times \Delta V^{(-8.840+0.895\times V_i)}$$

$$Sensor\ 2:\ F = 9.713 \times 10^{-4} \times \Delta V^{(-10.266+1.438\times V_i)}$$

$$Sensor\ 3:\ F = 1.923 \times 10^{-3} \times \Delta V^{(-9.057+1.112\times V_i)}$$

In the original *in vitro* experiments [17], the amplitude of the voltage pulse applied for heating was 8.2 V. The present experiments were conducted with a 9.6 V pulse, with the expectation that increasing the voltage amplitude would increase the temperature difference and thereby improve flow resolution. Based on first principles, the temperature rise is proportional to the square of the applied voltage; on average the temperature rise in the present experiments would be expected to be ~30% higher than in the previous *in vitro* experiments.

2.2. Animals and surgical procedures

Animal experimentation was approved by the Institutional Animal Care and Use Committee of the University of North Texas Health Science Center (protocol # IACUC-2017-0029) and was conducted in accordance with the *Guide to the Care and Use of Laboratory Animals* (U.S. National Research Council publication 85–23, revised 2011). Experiments were conducted in 8 juvenile Yorkshire swine (4 males) weighing 34–42 kg. After an overnight fast, the pigs were premedicated with telazol (6.7 mg/kg *im*) and xylazine (1.3 mg/kg *im*), intubated, and maintained under a surgical plane of anesthesia by mechanical ventilation (12–14 cycles/min; tidal volume 15 ml/kg) with 1–3% isoflurane in 100% O_2.

The animal preparation is shown in Fig. 2. Pigs were placed on a heated pad in the left lateral recumbent position, and body temperature was monitored via a rectal probe. Epidermal electrode patches were applied to the limbs to capture the standard lead II electrocardiogram. The mid-sagittal frontoparietal region of the

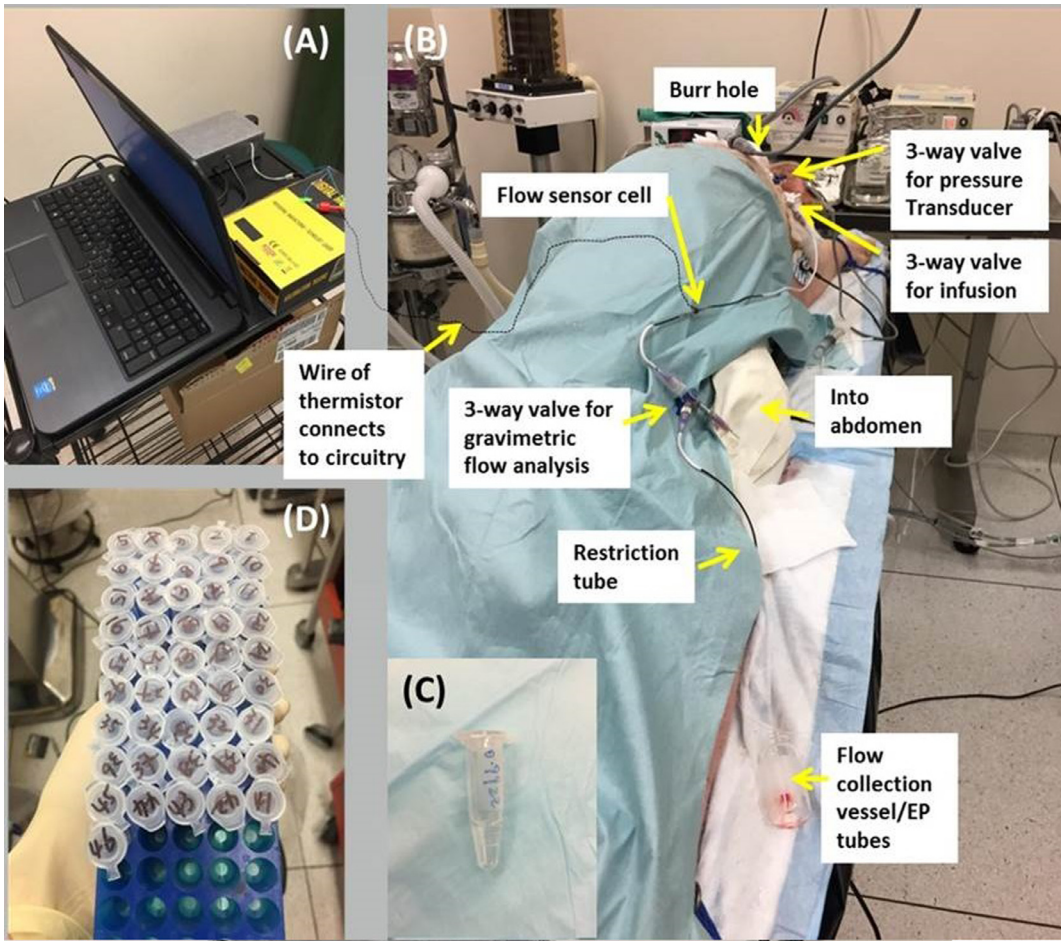

Fig. 2. Experimental setup for studies in anesthetized swine. (A) Shunt flow monitor and computer are located on a portable table on the left side of the operating table. (B) Top-rear view of the pig and flow system on the operating table. (C) A pre-weighed vial containing 5 min collection of CSF for gravimetric flow measurements is shown. (D) Vials are collected in a tray and are re-weighed after the experiment for gravimetric flow determination.

scalp was incised to expose the cranium. A 5 mm diameter burr hole was drilled approximately 5 mm to the right of the sagittal suture and 1 cm rostral to the frontal-parietal suture, and a vinyl catheter was inserted and advanced into the third cerebral ventricle. Catheter positioning in the third ventricle was verified by the spontaneous flow of straw-colored fluid into the catheter. After application of bone wax to seal the hole, the catheter was connected to a tubing to effect a ventriculoperitoneal shunt, via two 3-way stopcocks placed in series approximately 5–10 cm distal to the burr hole: one connected to a pressure transducer for monitoring cerebroventricular pressure, and the other for bolus injections of the artificial CSF described below. The distal end of the external shunt was inserted into the abdominal cavity for drainage.

An aqueous solution containing physiological concentrations of the major CSF electrolytes (141 mM Na^+, 120 mM Cl^-, 2.9 mM K^+ and 22 mM HCO_3^-) [20] was freshly prepared and maintained in a 37 °C water bath. This fluid was injected (5, 10, 15 or 20 ml bolus) into the cerebral ventricle via the cerebroventricular catheter.

2.3. Experimental protocol

The duration of experiments to evaluate flow sensor performance was 6–7 h. In-line sensors were installed at approximately the midpoint of the cerebroventricular-peritoneal tract. The sensor signal was transmitted via a thin wire (broken line in Fig. 2) to the flow monitor and laptop computer. To optimize detection of flow fluctuations, check valves were omitted from the shunt to avoid prolonged zero-flow periods [17]. A 3-way stopcock was placed in the shunt tract distal to the sensor, permitting diversion of shunt flow from the abdomen to a port permitting timed fluid collection for gravimetric flow analysis.

2.3.1. Tubing configurations

Opening or closure of stopcocks provided three different tubing configurations for flow measurement by the sensor, gravimetric flow measurement, and cerebroventricular injection of artificial CSF (Fig. 3). For sensor flow measurements, fluid flowed via the shunt from the third cerebral ventricle into the abdominal cavity. For concomitant sensor and gravimetric flow measurements, the shunt fluid was diverted through a restriction tube and collected in pre-weighed Eppendorf vials. The restriction tube (Fig. S4) had a smaller internal diameter than the shunt tube, enabling it to function as a shunt valve to provide constant flow restriction. This configuration permitted simultaneous sensor and empirical flow measurements to evaluate the sensor's performance. Artificial CSF (37 °C) was injected manually (5, 10, 15 or 20 ml bolus) into the cerebroventricular cannula. Injections were delivered at a steady rate over a 60 s period, during which the sensor continued to monitor shunt flow, but fluid collection for gravimetric analysis was suspended. There were 3–5 bolus injections over the course of each experiment. After each injection, shunt flow returned to baseline before the next injection. A solid-state pressure transducer (Digi-Med TXD-310, Micro-Med, Inc., Louisville, KY) was connected to the shunt via a stopcock. Cerebroventricular pressures

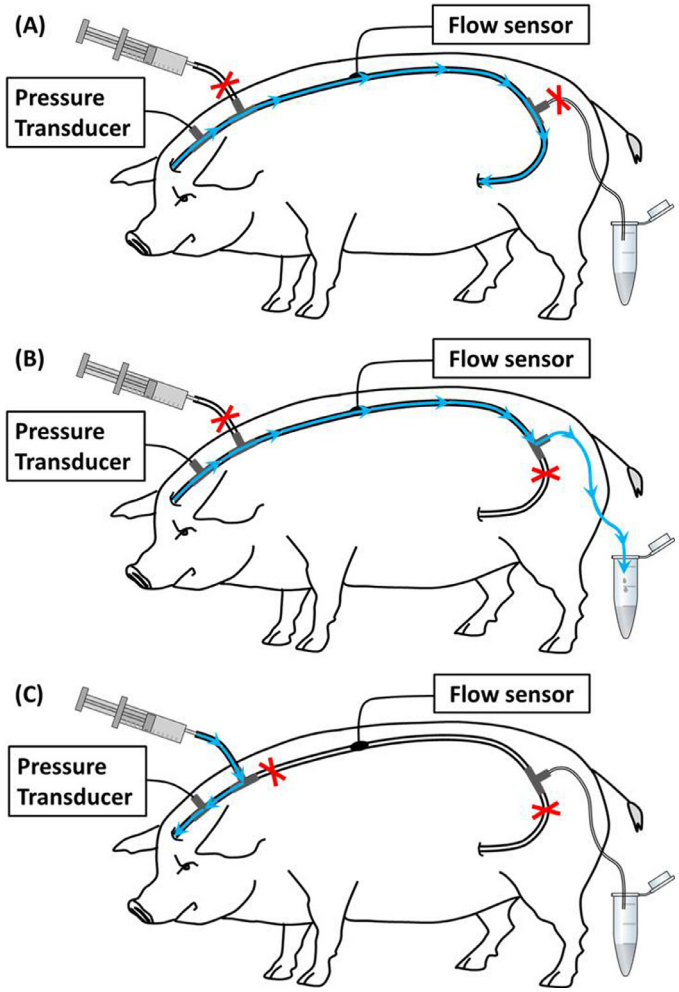

Fig. 3. Shunt flow and cerebroventricular pressure measurements. The blue arrows indicate flow direction, and the red crosses indicate the closed ports. (A) Shunt flow measurement by the in-line sensor during venting of CSF from cerebral ventricle to abdominal cavity. (B) Collection of CSF in pre-weighed vials through a restriction tube for gravimetric flow measurements. (C) Assessment of cerebroventricular pressure responses to injection of artificial CSF into the third cerebral ventricle. (For interpretation of the references to color in this figure legend, the reader is referred to the web version of this article.)

were monitored and recorded during the sensor and gravimetric flow measurements.

2.3.2. Sensor-reported flow

The flow sensor started reporting flows after the surgical preparation was completed and fluid was flowing through the shunt from cerebral ventricle to peritoneal cavity. The time of the first measurement was defined as $t = 0$ h. All other measurements were logged relative to this reference. Once started, the sensor continuously measured flows in 30 s segments until the end of the experiment. Each 30 s measurement cycle included 5 s for baseline sensing, 5 s for heating the shunt fluid at the sensor, and 20 s for measuring the flow-dependent decrease in fluid temperature. Fig. 4 presents the signal obtained over a typical measurement cycle.

A LabVIEW program automatically performed data analysis at the end of each cycle. V_i, V_f and ΔV were extracted, and then flow (F) was calculated from the calibration curves based on V_i and ΔV, and saved on an Excel spreadsheet. Because CSF shunt flow fluctuations in patients typically follow time courses lasting for hours [19], the sensor's flow measurements at 30 s intervals permit high-resolution detection and quantification of shunt flow fluctuations.

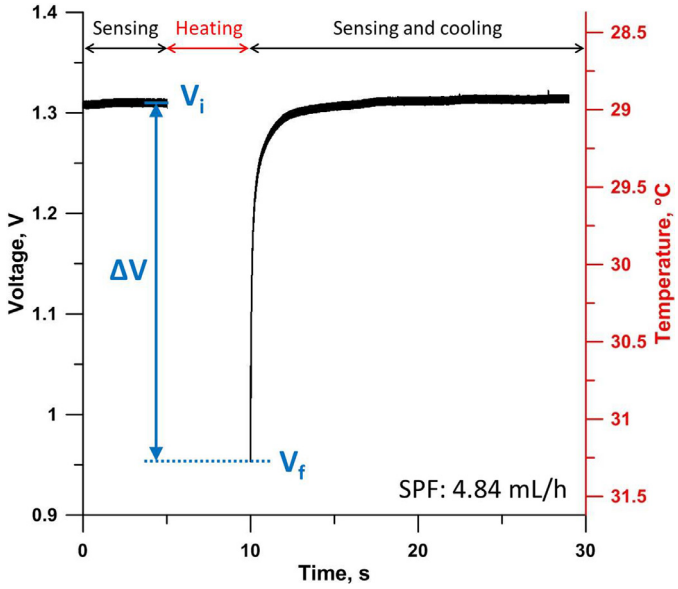

Fig. 4. Flow sensor voltage output of a single 30 s flow measurement cycle. Initial voltage V_i is defined as the average signal between 4.891 – 4.998 s. Final voltage V_f is the lowest voltage measured immediately after cessation of the 5 s heat pulse and reestablishment of the Wheatstone bridge. The difference ΔV (= V_i – V_f) is proportional to the shunt flow. Data collection continues from 10 to 30 s before initiation of the next cycle. This cycle reported SPF = 4.84 ml/h.

Table 1
Slopes and regression coefficients for linear regression analyses of gravimetrically measured (GMF) vs. sensor-reported (SRF) shunt flows.

Experiment #	Slope: GMF vs. SRF	SD	*r*
2	0.91	0.15	0.9476
3	1.20	0.23	0.7256
5	1.17	0.11	0.9612
6	1.13	0.18	0.9467
7	0.85	0.38	0.6200
8	1.01	0.11	0.9629

2.3.3. Gravimetric flow analysis

Flow was empirically determined by timed collection in pre-weighed Eppendorf vials of effluent from the restriction tube, while sensor-reported flow was monitored concomitantly. Effluent was collected for 5 min per vial, except during the first 10 min after artificial CSF injection, when fluid was collected for 60 s per vial. The vials were reweighed after the experiment. Effluent volumes were computed based on a CSF density of 1 g/ml [21,22]. Approximately 80–100 gravimetric flow measurements were made in each experiment.

2.4. Statistics

Microsoft Excel was used for all statistical analyses. The sensor-reported flows (SRF) were generated every 30 s while samples for gravimetric flow (GMF) measurements were collected for 1 or 5 min. The SRF data obtained over the duration of each GMF sample collection were averaged. Outliers were identified based on the SRF/GMF ratio, by the interquartile range (IQR) value. Data that fell below Q1-1.5*IQR or above Q3+1.5*IQR were discarded. The mean and standard deviation of the slope, as well as the correlation coefficient *r* are shown in Table 1; standard statistical functions in Excel were used. The SRF/GMF ratio in these experiments was 0.98 ± 0.09 (mean value ± SD, $n = 6$), and the 95% confidence interval was 0.88 - 1.07. The linear relationship between GMF as the independent variable and SRF as the dependent variable was examined by

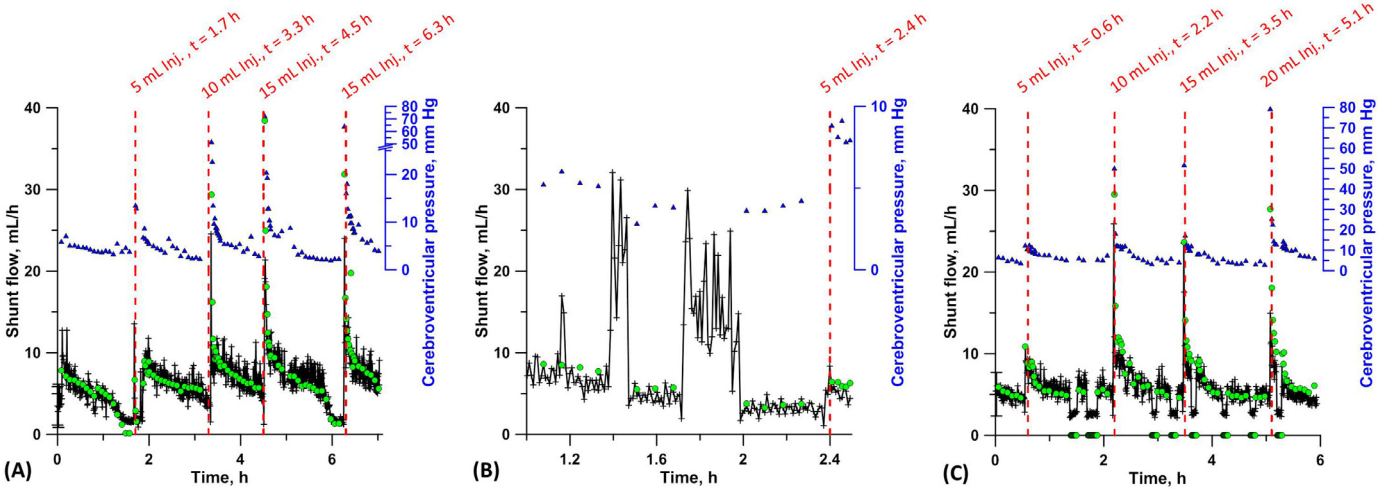

Fig. 5. Impact of bolus injections (vertical broken red lines) of artificial CSF on cerebroventricular pressures (blue traces) and temporal shunt flows determined by the flow sensor (black traces) and gravimetric measurements (green circles). (A) Flows and pressures during experiment 8. Volumes and times of intracerebral injections are indicated. (B) A 90 min portion of experiment 5 is shown to demonstrate the rapid response of the flow sensor to phasic changes in shunt flow following artificial CSF injections. (C) Values from experiment 6, in which the consistency of these zero-flow readings demonstrated a stable sensor baseline. (For interpretation of the references to color in this figure legend, the reader is referred to the web version of this article.)

standard linear regression methods with or without forcing the intercept through the origin. In no case could the intercept be statistically distinguished from zero, so further analyses examined best fit relationships with intercepts at the origin. These relationships yielded best fit slopes of 0.88 ± 0.01 (mean value ± SD, $n = 6$) and 95% confidence interval of 0.87–0.90.

3. Results and discussion

3.1. Sources of error and corrective measures

Two of the eight experiments did not produce processable data. In the first (Experiment 1), the sensor was pre-calibrated in the range of body temperature of the animal (32–39 °C). From the cranial entrance, the fluid travels ~35 cm through the shunt outside the body before passing through the sensor housing, and thus has an opportunity to cool towards ambient temperature. To maintain the fluid temperature within the calibration range, in the first experiment we covered the exposed tubing with a heating pad. However, the pad positioning in close proximity to the sensor electronics shifted the sensor response, producing erroneous flow values. A second problem stemmed from the absence of any restriction at the fluid exit during sample collection for gravimetric flow measurement, producing flows that exceeded the upper limit of reported CSF flows by up to fivefold. In subsequent experiments, these problems were solved by (a) calibrating the sensor around the ambient temperature range in which the sensor actually measured flow and (b) adding a restriction tube at the sampling port to limit the flow rate during gravimetric measurement. In Experiment 4, unknown to the experimenters at the time, the thermistor had a poor connection resulting in unpredictable and often subtle baseline shifts which impeded subsequent analysis of the SRF data. A new thermistor was utilized for the next set of experiments. The other 6 experiments yielded suitable flow signals.

3.2. Flow and pressure changes produced by artificial CSF injections

Fig. 5A presents shunt flows reported by SRF and GMF, and cerebroventricular pressures over the course of a typical experiment (Experiment 8). Altogether, 756 SRF and 108 GMF values were obtained over this 7.2 h experiment. At the beginning of the experiment, shunt flows ranged from 8–10 ml/h. Flows and cerebroventricular pressures gradually fell and eventually stabilized as CSF drained through the shunt. To test sensor performance at various flow rates, 5, 10 or 15 ml of artificial, pre-warmed (37 °C) artificial CSF electrolyte solution were injected into the third cerebral ventricle at 1.7, 3.3, 4.5 and 6.3 h. These injections produced abrupt flow surges and brief increases in cerebroventricular pressure that were roughly proportional to the injected volume. In the 6 experiments, pre-injection baseline cerebroventricular pressures averaged 3.3 ± 0.6 mm Hg (mean ± SEM). Injections of 5, 10, 15 and 20 ml produced peak pressure increases of 12.5 ± 2.5, 45 ± 6.2, 56 ± 5.3 and 74 ± 2.1 mm Hg, respectively. Thus, there was a roughly linear relationship between the injected fluid volume and the resultant increase in cerebroventricular pressure. These pressure increases were temporary and returned to baseline within 2–5 min as the injected volume exited the ventricle, either through the ventriculoperitoneal shunt or, as discussed below, via the normal anatomical drainage through the cerebral aqueduct and fourth ventricle.

In Experiment 5 (Fig. 5B), flow was diverted into the peritoneal cavity at $t = 1.3$ and 1.75 h. Because the ventriculoperitoneal shunt configuration imposed less resistance than the resistance tube drainage, shunt flow increased during these diversions. In each case, the sensor reported the flow surges promptly. In Experiment 6 (Fig. 5C), the shunt was clamped six times to temporarily interrupt flow, at 1.7, 2.9, 3.3, 3.7, 4.3, 4.7 and 5.2 h, and in each case, the flow sensor reported zero flow. At $t = 5.1$ h, a 20 ml artificial CSF injection produced a peak flow of 20 ml/h followed by a decline to 10 ml/h within 2–3 min. Thus, the injections produced temporary increases in cerebroventricular pressure and shunt flow that gradually subsided as the fluid drained.

A baseline shunt flow of 1.81 ± 0.26 ml/h/kg body mass was determined by GMF measurement. Analysis of the increased post-injection flow revealed that 28.7 ± 2.1% of the injected volume was recovered from the shunt; thus, approximately 70% of the injected fluid did not drain through the shunt. The experiments were conducted on healthy animals with anatomically intact CSF circulation, which very likely allowed most but not all of the injected fluid to pass from the third to the fourth ventricle, and ultimately into the subarachnoid space. The temporarily elevated cerebroventricular pressures produced by the injections would have increased this

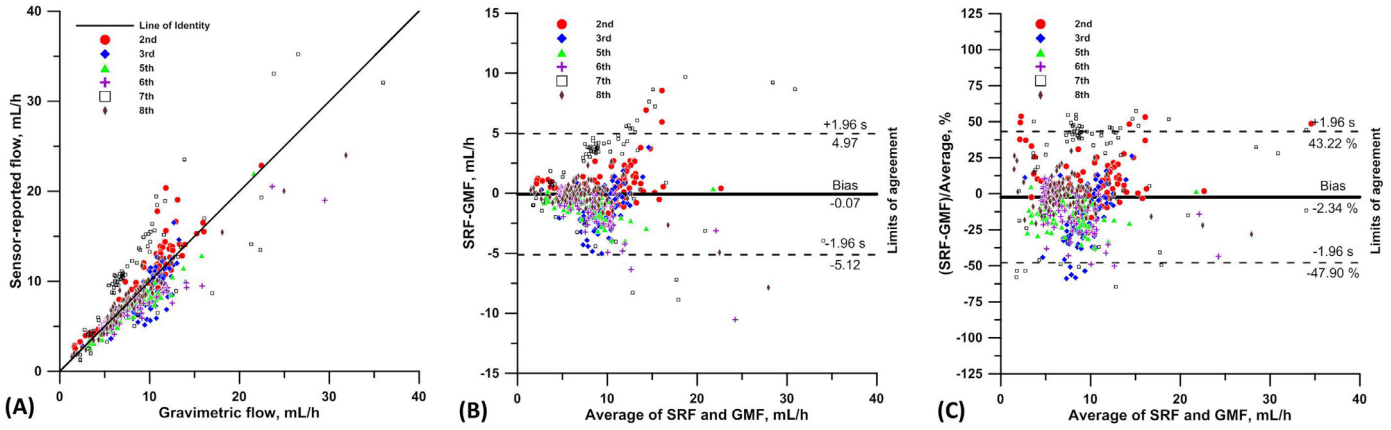

Fig. 6. Comparisons of flows reported by the sensor vs. gravimetric determination by (A) regression analysis, (B) Bland-Altman plot of the differences between the concurrent sensor and gravimetric values, and (C) Bland-Altman plot of differences presented as percentages of the mean flow values. In panel A, the different symbols represent data from each of the six experiments. The two flow measurements yielded robust correlations approximating the line of identity, where linear regression analysis of plotted data yielded $r^2 = 0.9412$. In panels B and C, the solid lines represent the mean value of the difference between sensor-reported and gravimetric flows, and the broken lines represent the upper and lower limits encompassing 95% of the individual differences.

natural CSF drainage, causing shunt flows to subside within a few min after injection. Supplemental Figure S5 shows the complete results of the six experiments.

3.3. Sensor calibration

Preliminary work showed no difference between sensor calibrations conducted with simulated CSF solutions vs. pure water; this may indeed be expected based on their virtually identical thermal properties. Sensor calibrations were therefore carried out with water, generating the data shown in Fig. S1 - S3. The sensor output during the actual experiments was translated to flow rates using such calibration data. The close correspondence of the SRF and GMF values in the animal experiments suggests water can serve as a convenient flow calibrant. The sensor baseline output fluctuated in synchrony with the respiratory rhythm of the animal (Fig. S6); this can be ascribed at least in part to CSF flow changes associated with fluctuations in cerebroventricular pressure during positive-pressure, mechanical ventilation [23,24]. Despite these fluctuations, the sensor generated accurate flow metrics.

3.4. SRF and GMF comparison

Fig. 6A presents a scatter plot of the values reported by the SRF vs. GMF methods. A total of 506 pairs of SRF and GMF data obtained simultaneously from six experiments are shown. Least-squares linear regression correlation coefficients for individual experiment were between 0.88 and 0.99, indicating robust concordance of SFR and GMF. Although some variation around the line of identity was observed, the average SRF/GMF ratio was 0.98 ± 0.09, and the 95% confidence range of 0.88–1.07 encompassed unity, indicating the sensor accurately measured shunt flow.

The accuracy of SRF was further examined by a Bland-Altman plot, where the differences between the two paired measurements are plotted against the average (Fig. 6B). On average, GMF reports flows only 0.07 ml/h above SRF, indicating the sensor accurately reported shunt flow. The Bland-Altman plot revealed widening of the SRF-GMF difference at higher flows, suggesting the variability of the difference is not constant. When the differences are expressed as percentages of the mean of SRF and GMF, the data scatter is nearly constant over a broad flow range (Fig. 6C). The two methods showed robust agreement from a statistical point of view, but from a clinical standpoint, little information is presently available about the acceptable limits of shunt flow measurement. Currently available hydrocephalus diagnostics provide only “on/off” information about CSF flow; consequently, the intermittence of CSF flow [25] may produce false findings. The sensor’s robust detection of shunt flow in the present study suggests this technology may eventually afford greater reliability and precision than current methods for clinical assessment of shunt performance.

3.5. Choice of pulse voltage

In retrospect, the choice of using a 9.6 V pulse compared to the original 8.2 V operation was unwise. Although there was no obvious indication of malfunction (the signal returned to baseline before the next pulse) the devices apparently did suffer from the added thermal stress. *Post-hoc* examination of the data indicates that the sensors performed well for two experiments plus added calibration runs at 9.6 V, but began to falter by the third experiment and failed by the fourth. When 8.2 V pulses were applied in vitro, the sensors performed reliably without functional deterioration [17].

4. Conclusions

We have demonstrated the functionality of a previously reported hydrocephalus shunt flow sensor in anesthetized pigs. More than 4300 acceptable flow measurements were taken in six acute experiments. The sensor proved to accurately report flow of porcine CSF at ambient temperatures. The shunt and sensor were placed externally to permit gravimetric flow measurements; a crucial next step in development will be to interrogate the long term performance of the sensors when implanted subcutaneously in chronically instrumented animals, using wireless communication and instrument control technology. Application of higher voltage pulses produced minimal enhancement of flow resolution and adversely affected sensor longevity. Accordingly, future experiments will utilize electrical pulses $\leq$ 8.2 V.

Acknowledgments

This work was supported by the Texas Medical Research Consortium (TXMRC). The outstanding technical support of Shirley Nelson, R.L.A.T. (UNTHSC Department of Lab Animal Medicine) and Thomas Medrano (St. Mary’s University, San Antonio, TX) is gratefully acknowledged. We thank Dr. Aditya N. Das (University of Texas at Arlington Research Institute) for his expert assistance with

the sensor electronics. The authors declare no competing interests. Ethical Approval: UNTHSC protocol #IACUC-2017-0029.

Disclosure

The authors report no conflict of interest concerning the materials or methods used in this study or the findings reported in this article.

Supplementary materials

Supplementary material associated with this article can be found, in the online version, at doi:10.1016/j.medengphy.2019.03.010.

References

[1] Tully HM, Capote RT, Saltzman BS. Maternal and infant factors associated with infancy-onset hydrocephalus in Washington State. Pediatr Neurol 2015;52:320–5.
[2] Tully HM, Dobyns WB. Infantile hydrocephalus: a review of epidemiology, classification and causes. Eur J Med Genet 2014;57:359–68.
[3] Simon TD, Riva-Cambrin J, Srivastava R, Bratton SL, Dean JM, Kestle JR. Hydrocephalus clinical research network. Hospital care for children with hydrocephalus in the United States: utilization, charges, comorbidities, and deaths. J Neurosurg Pediatr 2008;1:131–7.
[4] Waziri A, Fusco D, Mayer SA, McKhann GM, Connolly ES Jr. Postoperative hydrocephalus in patients undergoing decompressive hemicraniectomy for ischemic or hemorrhagic stroke. Neurosurgery 2007;61:489–94.
[5] Leinonen V, Vanninen R, Rauramaa T. Cerebrospinal fluid circulation and hydrocephalus. Handb Clin Neurol 2017;145:39–50.
[6] Hallaert GG, Vanhauwaert DJ, Logghe K, Van den Broecke C, Baert E, Van Roost D, Caemaert J. Endoscopic coagulation of choroid plexus hyperplasia. J Neurosurg Pediatr 2012;9:169–77.
[7] Martínez-Lage JF, Pérez-Espejo MA, Almagro MJ, López-Guerrero AL. Hydrocephalus and arachnoid cysts. Child Nerv Syst 2011;27:1643.
[8] Bu Y, Chen M, Gao T, Wang X, Li X, Gao F. Mechanisms of hydrocephalus after intraventricular haemorrhage in adults. Stroke Vasc Neurol 2016;1:23–7.
[9] Yamasaki M, Nonaka M, Bamba Y, Teramoto C, Ban C, Pooh RK. Diagnosis, treatment, and long-term outcomes of fetal hydrocephalus. Semin Fetal Neonatal Med 2012;17:330–5.
[10] Wright Z, Larrew TW, Eskandari R. Pediatric hydrocephalus: current state of diagnosis and treatment. Pediatr Rev 2016;37:478–90.
[11] Chumas P, Tyagi A, Livingston J. Hydrocephalus—what's new? Arch Dis Child Fetal Neonatal Ed 2001;85:F149–54.
[12] Drake J, Kestle J, Milner R, Cinalli G, Boop F, Piatt J Jr, Haines S, Schiff SJ, Cochrane DD, Steinbok P, MacNeil N. Randomized trial of cerebrospinal fluid shunt valve design in pediatric hydrocephalus. Neurosurgery 1998;43:294–303.
[13] Stein SC, Guo W. Have we made progress in preventing shunt failure? A critical analysis. J Neurosurg Pediatr 2008;1:40–7.
[14] Othman A, Hamou HA, Pjontek R, Afat S, Clusmann H, Wiesmann M, Brockmann MAl. Evaluation of whole body Ultralow-Dose CT for the assessment of ventriculoperitoneal shunt complications: an experimental ex-vivo study in a swine model. Eur Radiol 2015;25:2199–204.
[15] Kahle KT, Kulkarni AV, Limbrick DD Jr, Warf BC. Hydrocephalus in children. Lancet 2016;387:788–99.
[16] Madsen JR, Abazi GS, Fleming L, Proctor M, Grondin R, Magge S, Casey P, Anor T. Evaluation of the ShuntCheck noninvasive thermal technique for shunt flow detection in hydrocephalic patients. Neurosurgery 2011;68:198–205.
[17] Qin C, Stamos B, Dasgupta PK. Inline shunt flow monitor for hydrocephalus. Anal Chem 2017;89:8170–6.
[18] Medtronic Neurosurgery P.S. Medical CSF-Flow Control Valves, instructions for use. 2008;13651-1 G 21251.
[19] Kadowaki C, Hara M, Numoto M, Takeuchi K, Saito I. CSF shunt physics: factors influencing inshunt CSF flow. Childs Nerv Syst 1995;11:203–6.
[20] Damkier HH, Brown PD, Praetorius J. Epithelial Pathways in choroid plexus electrolyte transport. Physiology 2010;25:239–49.
[21] Levin E, Muravchick S, Gold M. Density of normal human cerebrospinal-fluid and tetracaine solutions. Anesth Analg 1981;60:814–17.
[22] Lui ACP, Polis TZ, Cicutti NJ. Densities of cerebrospinal fluid and spinal anaesthetic solutions in surgical patients at body temperature. Can J Anaesthesia 1998;45:297.
[23] McGuire G, Crossley D, Richards J, Wong D. Effects of varying levels of positive end-expiratory pressure on intracranial pressure and cerebral perfusion pressure. Crit Care Med 1997;25:1059–62.
[24] Videtta W, Villarejo F, Cohen M, Domeniconi G, Santa Cruz R, Pinillos O, Rios F, Maskin B. Effects of positive end-expiratory pressure on intracranial pressure and cerebral perfusion pressure. Acta Neurochir Suppl 2002;81:93–7.
[25] Marlin AE, Gaskill SJ. The use of transcutaneous thermal convection analysis to assess shunt function in the pediatric population. Neurosurgery 2012;70(suppl 2):181–3.